DIRECT OBSERVATION OF DENSIFICATION AND GRAIN GROWTH IN A W-Ni ALLOY

Helmut Riegger*, Joseph A. Pask and H. E. Exner**

Materials and Molecular Research Division, Lawrence Berkeley Laboratory
and Department of Materials Science and Mineral Engineering,
University of California, Berkeley CA 94720

ABSTRACT

Densification and grain growth in a tungsten-nickel alloy containing 32 vol % of liquid at 1550°C were studied by conventional methods aided by hot stage scanning electron microscopy and cinematography. This technique yields important additional qualitative information on the mechanisms. Two stages can be discerned. In stage 1, essentially complete pore elimination, rapid grain growth and adjustment of microstructural geometry take place. In the second stage, microstructure coarsening occurs which is characterized by geometric similarity. Columnar grain growth at the surface is observed due to squeezing out of Ni-W liquid, flooding of surface grains and fast evaporation of the Ni. The driving forces for these processes are discussed showing that a high ratio of grain boundary energy to liquid surface energy is essential. A W-Cu alloy with 32 vol % liquid at 1100°C did not show any grain growth due to essentially no solubility of W in Cu at this temperature.

*Present address: Brown Boveri Research Center, Baden, Switzerland.

**Present address: Max-Planck-Institut für Metallforschung, Institut für Werkstoffwissenschaften, Stuttgart, Germany.

INTRODUCTION

Densification and particle growth in the heavy metal systems (tungsten with nickel, copper or iron) have been studied extensively. Following the classical work by Price, Smithells and Williams[1], numerous papers have been published describing the phenomenology and the kinetics of the processes occurring during sintering.[2-9] Frequently, the classical theories of liquid-phase sintering,[10] and Ostwald ripening[11,12] were applied for quantitative evaluation of the shrinkage and particle growth behavior. However, due to the complexity introduced by interaction of these processes with additional processes going on during the entire heating cycle, no clear picture exists on the mechanisms by which the final microstructure of heavy metals is formed.

In this paper, additional evidence is presented relative to the complexity of the processes by means of continuous monitoring and filming of the development of the microstructure of W-Ni and W-Cu alloys in a hot stage scanning electron microscope. These observations in combination with well known metallographic procedures provides a deeper insight into the mechanisms of densification and particle growth of heavy metal systems.

EXPERIMENTAL PROCEDURES

Spherical W powder (Fig. 1) of 99.8 wt% purity with an average particle size of 4μm was mixed with spherical nickel powder (99.9 wt%, average particle size 40μm) and spherical copper powder (99.9 wt%, 44μm) to give the following compositions: a) 92 wt% W - 8 wt% Ni, and b) 82 wt% W - 18 wt% Cu. At the isothermal test temperatures used (1550°C for the W-Ni and 1100°C for the W-Cu alloys), the amount of liquid phase

is 32 vol % in both systems. These figures take into account the substantial solubility of W in molten Ni and essentially no solubility of W in molten Cu. Good mixing was achieved by tumbling a slurry of these mixtures with ethyl alcohol in a rotating rack for 24 hours. After drying, the mixed powder was examined microscopically and was found to have a uniform distribution of the lower melting metal.

Cylindrical specimens (5mm diameter, 4mm length) were pressed in a non-lubricated die at a pressure of 70 MPa resulting in a green density of 63% of the theoretical density.

Heat treatment was carried out in the hot stage of a scanning electron microscope in a vacuum of approximately 3 Pa. The design and operation of the hot stage has been described previously.[13] The instrument allows direct observation of the sample surface up to 1700°C. Nominal magnification was 1000X in most cases, and videotape recording or filming was carried out with speeds of 0.1 to 1 frames per second.

For all samples, the following heating cycle was used: heating to 900°C in 10 min, isothermal treatment for temperature equilibration for 5 min and heating to the isothermal test temperature at 20°C/min. The W-Ni samples were then held at 1550°C, and the W-Cu samples at 1100°C for various test times.

Mean linear intercepts were measured from the recorded videotapes as well as from metallographically polished and etched cross sections. Near identical results were obtained. The microstructural analysis was carried out using simple devices (a ruler and a protractor). Standard stereological parameters (mean linear intercept, intercept length distribution, specific surfaces, contiguity and dihedral angles) were

determined. Though there may be a range of dihedral angles, no attempt was made to derive this value from the apparent distribution of dihedral angles. The modes of the angle distribution was taken to correspond to the true angle. Lineal counting was carried out along traverses with 2000μm total length. At least 500 intercepts were measured for each sample and recorded in classes of 1μm width. The size distributions were normalized with respect to the mean linear intercept and to total number of intercepts measured to be able to evaluate shape changes of the distribution curve. This procedure causes class width to vary with mean linear intercept (compare data in Fig. 8). Densities were recorded by buoyancy measurements.

RESULTS

Figure 2 shows a scanning electron micrograph of the fracture surface of the W-Ni powder mixture heated to 1100° and held for 30 min. The formation of necks is clearly revealed and dihedral angles can be seen. This structure corresponds to that observed in Ni- activated sintering of tungsten where pronounced neck formation at temperatures shortly above 1000°C and dihedral angles of 35 degrees[14] were observed. Most of the tungsten particles are single crystals in this stage. Figure 3 shows a series of scanning micrographs taken at room temperature from the surface of the sintered samples. Shortly after appearance of liquid (Fig. 3a), clusters of tungsten grains form. These grains grow rapidly with time in the way shown in Figs. 3b to 3d. For comparison, an SEM micrograph of a cross-section of the sample sintered for 20 min at 1550°C is shown in Fig. 4a. Figure 4b shows a cross-section normal to the surface. Columnar grain growth near the surface is

clearly visible. It is interesting to note that the grain size measured parallel to and at the surface is comparable to that in the interior in spite of this obvious shape difference. It is of further interest to note that no necks were observed after the Ni melted and became saturated with W.

Pictures taken at temperature (Fig. 5) from the TV screen are less sharp. They show, however, an unexpected phenomenon which is even much more clearly revealed in the movies taken: some of the grains suddenly turn black and then gradually get light gray again. Tungsten saturated nickel melt is squeezed out from the sample through channels and spreads over one of the grains. In a few seconds (compare Figs. 5a and 5b) the nickel vaporizes leaving a layer of tungsten behind. This process occurs repeatedly and discontinuously at different locations on the surface resulting in the structure shown in Fig. 4b.

Figures 6 to 10 show the changes of density and microstructural geometry with time at 1550°C. Density (Fig. 6) increases rapidly to about 17.7 g/cm^3, which is near the theoretical density of the W-8 wt% Ni alloy (approx. 17.65 g/cm^3 assuming that the atomic volume of tungsten does not change during solution in nickel). Upon further sintering, density increases slowly, obviously due to the evaporation of nickel. Grain size (Fig. 7) follows the same pattern. There is a discontinuity of grain growth after ~2 min of isothermal sintering: the grain growth rate decreases more or less discontinuously to a value lower by a factor of 20 and then stays nearly constant up to 30 min. This figure also shows that no grain growth occurs in the W-Cu system with an approximately equal volume of liquid phase reflecting the essential role of solubility.

Figure 8 shows the normalized grain size distributions for the tungsten grains for various sintering times at 1550°C. The width of the size range first decreases, then increases again and remains constant from 3 to 30 min indicating stationary shape. The specific interfaces S_{W-W} and $S_{W-Ni[W]}$ were measured as a function of annealing time from the microstructure of the samples. A continuous decrease of the W-liquid phase interface areas has been observed. However, the values for the W-W interfaces level off after about 5 minutes and remain fairly constant (Fig. 9). Contiguity, defined as the ratio of grain boundary area to total surface area of the tungsten grains, drops from an initially high value to a minimum, increases slightly, and then remains constant (Fig. 9).

Figure 10 demonstrates that the initially high dihedral angle (approximately 38 deg.) reaches an equilibrium value of approximately 8 deg. within 3 min which corresponds to the time taken to reach a minimum in the contiguity curve of Fig. 9. The fracture surface indicates mostly a fracture through the matrix showing the flat W-W interfaces and the W-liquid phase interfaces (Fig. 11a). A few regions with intergranular fractures have also been found (Fig. 11b). This seems to indicate varying adhesion at the interfaces, an interesting fact which was not followed up in this paper.

DISCUSSION

The results indicate the existence of two stages* in the isothermal sintering process after the formation of liquid. The amount of liquid is sufficient to essentially fill all the pores at the end of the first stage. Density changes and grain growth occur rapidly during this stage, and grain size distribution and dihedral angles are adjusting to stationary values. This stage ends rather abruptly after approximately 2-3 min. In the second stage, density and grain size increase much more slowly and the microstructure shows geometric similarity throughout this stage, i.e. the shape of the grain size distribution, contiguity and dihedral angle (as well as other nonmetric geometrical properties) remain constant. The interesting feature in this stage is the increase of density in spite of the fact that essentially all pores have been eliminated during the first stage. This effect occurs due to vaporization of Ni.

Stage 1. The fast shrinkage to full density is obviously related to the high solubility of tungsten in liquid nickel and the high driving force supplied by the surface energy of the nickel melt which causes rearrangement of W particles. The W-Cu system, in which there is no solubility of W in molten Cu, does not undergo the rearrangement of particles and stays porous even after long sintering times. This stage has usually been neglected in grain growth studies. Most often the

*It should be emphasized that these two stages are different from those discussed by Kingery[10] and others for densification in liquid phase sintering in which the amount of liquid on formation is not sufficient to fill all the pores so that the second stage is a densification stage due to elimination of remaining pores.

trends observed at longer sintering times have been extrapolated to the early times. This may lead to serious errors in the evaluation of grain growth kinetics by taking the slope of the grain size – time plot in logarithmic coordinates without making the proper corrections for zero time. As described earlier,[9,14] fast grain growth can occur due to preferential dissolution of particles with high internal stresses and reprecipitation on adjacent particles with a smaller amount of internal stresses. Though no experiments were carried out to evaluate the degree of deformation and internal stresses in the fine tungsten powder used, the high grain growth rate in Stage 1 can be attributed to this mechanism. Additionally, coalescence (coarsening by grain boundary movement aided by dissolution and reprecipitation to adjust the particle shape) can take place, again with internal stresses as an additional driving force. Accordingly, the area of grain boundaries formed during sintering prior to the formation of liquid is reduced rapidly in this stage.

The decrease of the dihedral angle is another interesting phenomenon. EDAX-analysis of the binder phase shows that Ni is saturated with W shortly after melting occurs, i.e. during the first half minute. Thus, interfacial energies are constant later in the process and the angle change is due to the gradual approach to the equilibrium value. Figure 2 clearly shows that necks form between the tungsten particles during heating up period before a liquid phase occurs. According to Gessinger and Fischmeister,[15] the equilibrium dihedral angle during Ni-activated solid state sintering of tungsten is 35 deg. This value agrees very well with the one observed here shortly after melting (approx. 38 deg., see Fig. 10). Then, during grain growth, new dihedral angles are

formed gradually shifting the observed maximum frequency value (mode) of the distribution towards the equilibrium dihedral angle which is in the order of 8 deg. in this system. With decreasing dihedral angle the ratio of grain boundary area to interfacial area decreases as reflected by the decrease of contiguity in Stage 1 (Fig. 9).

The adjustment of the grain size distribution towards a stationary shape (Fig. 8) was earlier observed by other authors[3,4] and can be visualized as follows. The wide size distribution of the initial powder rapidly narrows since all small particles are dissolved when the liquid approaches its equilibrium composition and no small grains are reformed. On the other hand, Ostwald ripening occurs after the liquid is saturated. Coarsening is then due to dissolution of material from small and reprecipitation on large particles. Small grains thus are formed again from larger ones and a stationary size distribution appears which has a shape very close to that predicted for linear intercept distributions derived from theoretical treatment of Ostwald ripening;[16] but there is an additional tail at large particle sizes which, in our opinion, is due to the fact that further coalescence takes place at this high volume fraction of the dispersed phase.

Stage 2. The transition from the first to the second stage is marked by the following features of microstructural geometry: Porosity has been eliminated to a degree that only a few small pores are left. The microstructure has assumed a dynamic equilibrium configuration with respect to the shape of the interfaces and to size distribution, and further changes can be described by increasing the scale of all metric properties by a constant factor. There is, however, one important

deviation from geometric similarity; the volume fraction of liquid (or nickel phase) decreases as is obvious from the density increase (Fig. 6) which characterizes this stage of liquid phase sintering.

The decrease of the liquid could be considered to be a continuous evaporation from the available liquid surface with a corresponding shrinkage of the compact. This explanation is, however, not sustained by the evidence given by hot stage SEM cinematography; spreading of liquid on the grains indicates that more liquid is squeezed out than evaporates from the available liquid/atmosphere area. Thus, the driving force for this process must be found in the interior of the specimen.

It has been shown[17] that a specific geometric configuration may become stable in a sintering system when the energy released by a reduction of the solid/liquid interface area is matched by the energy necessary to create new grain boundary area. This configuration manifests itself by an equilibrium dihedral angle and by interfaces of minimum area. This situation seems to have been locally reached in Stage 2. However, there are several reasons that it may be energetically more favorable to decrease the amount of liquid.

1. Let us consider a simple planar configuration as shown in Fig. 12 in which the liquid regions are assumed to have an equilibrium shape with dihedral angles of $\theta = 60$ deg. This corresponds to a ratio of grain boundary energy to solid-liquid interfacial energy of $\frac{\gamma_{SS}}{\gamma_{SL}} = \sqrt{3}$ substituted by solid and the liquid region is thus reduced in size with no change in configuration, the change of total interfacial energy for each liquid region is zero as shown in Eq. (1).

$$\Delta F = 3\,\gamma_{SL}\,a - 3\,\gamma_{SS}\,\frac{2}{\sqrt{3}}\cdot\frac{1}{2}\,a = 3\,\frac{\gamma_{SS}}{\sqrt{3}}\,a - 3\,\frac{\gamma_{SS}}{\sqrt{3}}\,a = 0 \qquad (1)$$

This does not provide a driving force for closure. However, when the solid material fills the liquid pore region by transport from the grain boundaries to the pores and the liquid material is squeezed out, the resulting grain edge length A_2 is shorter than A_1. The total negative energy change for one grain (6 sided as shown in example) taking into account Eq.(1) then is given by Eq.(2)

$$\Delta F = \frac{6}{2}\,\gamma_{SS}\,(A_2 - A_1) \qquad (2)$$

which constitutes a positive driving force for the reduction of the size of the liquid regions. A similar argument holds for the shrinkage of three dimensional liquid regions for any value of γ_{SS}/γ_{SL} and the corresponding minimum interface configurations.[18] Then, if a mechanism is available to reduce the amount of liquid, i.e., if there are channels open to the surface, solid material will diffuse from the grain boundaries to the liquid regions and the squeezing out of liquid will take place. In a non-homogeneous system there would also be regions in which equilibrium dihedral angles had not yet been reached which would also provide a driving force for closure.

2. During coalescence, grain boundaries break away from their positions at the dihedral angle grooves (Fig. 13). Then, the shape of the liquid region changes by solution and reprecipitation. Thereby, the dihedral angle deviates from its equilibrium value. In this situation, material can flow out from the grain boundary since reverse curvatures cause compressive stresses. Again, if there are channels to the

surface, the liquid will be squeezed out.

There is, however, another factor to be considered. The surface tension of the liquid results in a back-driving force as shown in Fig. 14. Only if the internal pressure of the liquid due to the mechanisms discussed above is larger than the critical pressure $2\gamma_{LV}/r_c$ (where r_c is the radius of curvature of the hemispherical droplet formed on the surface (Fig. 14c) and γ_{LV} is the surface energy of liquid), shrinkage of the liquid regions can go on. Since the driving force for this shrinkage is proportional to the grain boundary energy γ_{SS}, the process requires a sufficiently high ratio of γ_{SS}/γ_{LV}. In the tungsten-nickel system, this ratio is especially favorable. According to Gessinger et al.[19] γ_{LV} for nickel is 0.67 J/m^2. γ_{SS} can be estimated from the grain boundary grooving angle θ_{SSV}, the dihedral angle θ_{SSL} and the wetting angle θ_{SLV}. θ_{SV} and θ_{SSL} were found to be 38 and 8 deg. respectively (see Fig. 10); θ_{SLV} was taken from an earlier paper[20] to be 8 deg. Then we obtain Eq.(3).

$$\gamma_{SS} = 2\gamma_{LV} \cdot \frac{\cos\theta_{SSV}/2 \cdot \cos\theta_{SSL}/2 \cdot \cos\theta_{SLV}}{\cos\theta_{SSL}/2 - \cos\theta_{SSV}/2} =$$

$$2 \cdot 0.67 \cdot \frac{\cos 19 \cdot \cos 4 \cdot \cos 8}{\cos 4 - \cos 19} \approx 24 \ J/m^2 \qquad (3)$$

This surprisingly high value should only be taken as an indication for the high grain boundary energy of nickel-doped tungsten. This fact is generally supported by the small θ_{SSL}. For other systems, e.g. WC-Co or Fe-Cu, squeezing out of liquid has not been observed. In these cases, the ratio of γ_{SS}/γ_{LV} can be assumed to be much smaller and, as shown in Fig. 14f, evaporation can then only take place from the negatively

curved surfaces at the end of the liquid channels.

As soon as the squeezed out liquid assumes a hemispherical shape (Fig. 14c), further increase of liquid reduces the radius of curvature (Fig. 14d). Thus, the back pressure is released and the liquid spreads over a favorably located grain. This spreading may be aided by the existence of the small pores in which the vapor pressure builds up in accordance with the decreasing liquid surface curvature (Figs. 14a to c) and then is suddenly released yielding a discontinuous push-out of liquid in the stage shown in Fig. 14d. Then, the droplet spreads (Fig. 14e), evaporation takes place (Fig. 14f) and the cycle starts again.

The squeezing out of the liquid stops when the channels to the surface are pinched off which is analogous to the development of closed pores. This does not occur until later in the process. In the experiments described here open channels existed up to the longest sintering times used (30 min). Since the density of the vaporizing nickel is smaller than that of the tungsten, the density of the alloy increased (Fig. 6). Obviously, no density change or a density increase would be observed if the vaporizing species had the same or a higher density than the sample.

CONCLUSIONS

1. During heating of W-Ni, activated sintering of tungsten occurs. After formation of a liquid phase, two stages can be distinguished in the development of the microstructure.

2. In the first stage, porosity is eliminated and microstructural geometry changes drastically due to a sufficient amount of Ni. Rapid grain growth occurs due to solution and coalescence of W particles

driven by varying internal strains in the tungsten particles.

3. In the second stage, microstructural geometry is characterized by a constant dihedral angle, a stationary size distribution and nearly constant contiguity. Slow grain growth occurs, the kinetics of which follow the pattern described in earlier investigations. Microstructures are geometrically similar throughout this stage.

4. The essential feature in Stage 2 is the density increase due to nickel evaporation. The process allowing for rapid evaporation (squeezing out and discontinuous flooding of surface grains) has been explained by simple thermodynamic considerations.

5. Columnar grain growth at the surface is due to the discontinuous deposition of tungsten on flooded grains when the nickel vaporizes.

ACKNOWLEDGMENT

Grateful thanks are extended to D. J. Miller for many helpful discussions.

This work was supported by the Division of Materials Sciences, Office of Basic Energy Sciences, U.S. Department of Energy under contract No. W-7405-Eng-48. The Rotary Foundation granted a Fellowship to the senior author.

FIGURE CAPTIONS

Fig. 1. Spherical W powder with average grain size of 4μm.

Fig. 2. SEM of fracture surface of W-Ni powder heated to 1100°C and held for 30 min.

Fig. 3. Scanning micrographs of surfaces of sintered samples that were held at 1550°C for (a) 20 sec, (b) 2 min, (c) 10 min, and (d) 20 min.

Fig. 4. Scanning micrographs of polished cross-sections of samples sintered for 20 and 30 min at 1550°C: (a) parallel to surface, and (b) normal to surface.

Fig. 5. SEM photographs taken from surface at 1550°C ten seconds apart.

Fig. 6. Density of W-Ni compact vs time at 1550°C.

Fig. 7. Average grain size vs time for W-Ni compacts at 1550°C and W-Cu compacts at 1100°C.

Fig. 8. Normalized grain size distributions for the tungsten grains for various sintering times at 1550°C.

Fig. 9. Specific boundary areas (W-W and W-Ni) and continuity in W-Ni compacts with increasing sintering time.

Fig. 10. Dihedral angle ranges after 20 sec, 60 sec and 3-30 min at 1550°C.

Fig. 11. SEM photographs of several fracture surfaces of specimens sintered for 20 min.

Fig. 12. Schematic of microstructure with liquid at triple points transformed to one with elimination of liquid phase.

Fig. 13. Schematic of change of configuration of pore due to grain boundary break away.

Fig. 14. Schematic of flow of liquid from capillary channel onto surface of specimen. Internal pressure must overcome surface tension of liquid.

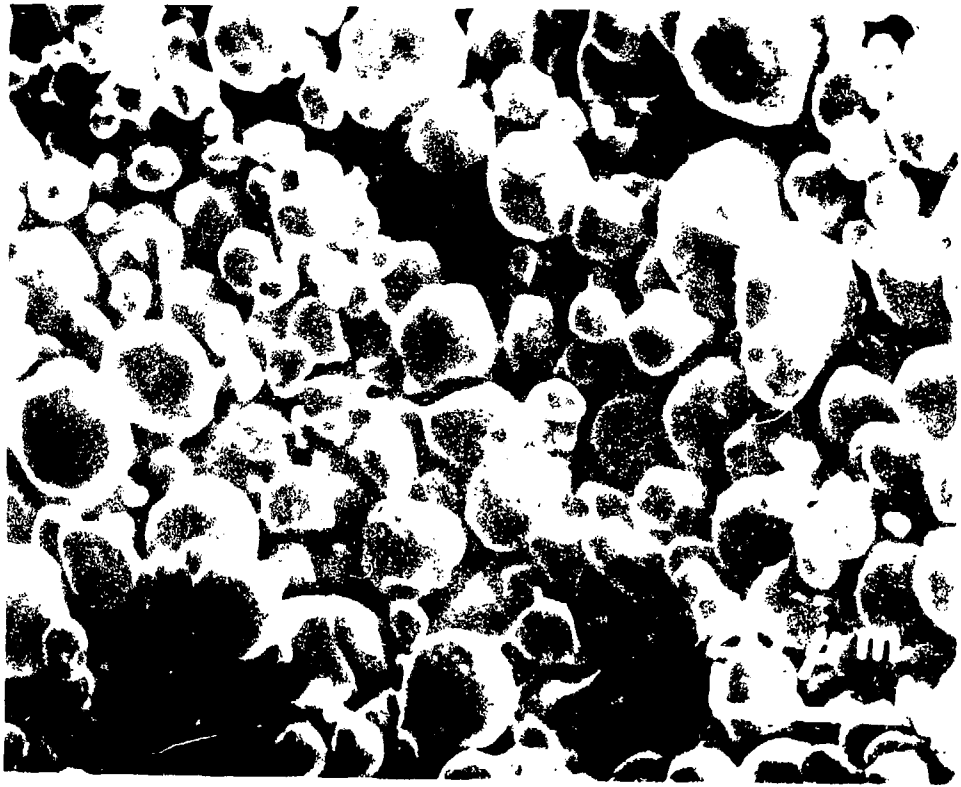

XBB 795-6881-A

Fig. 1

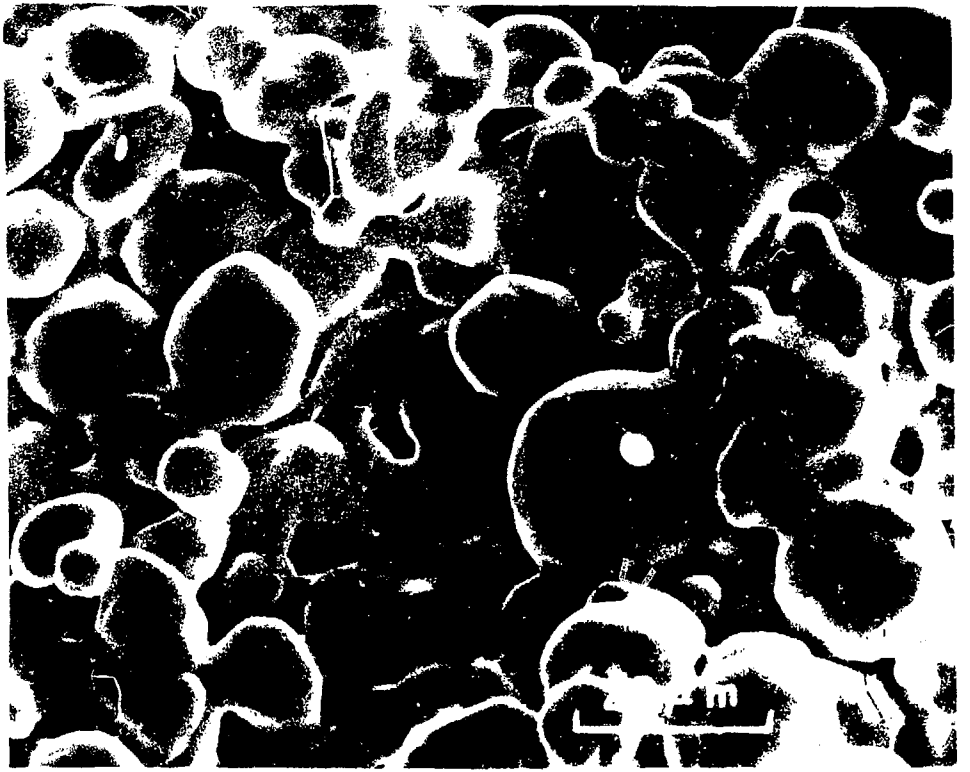

XBB 795-6881-B

Fig. 2

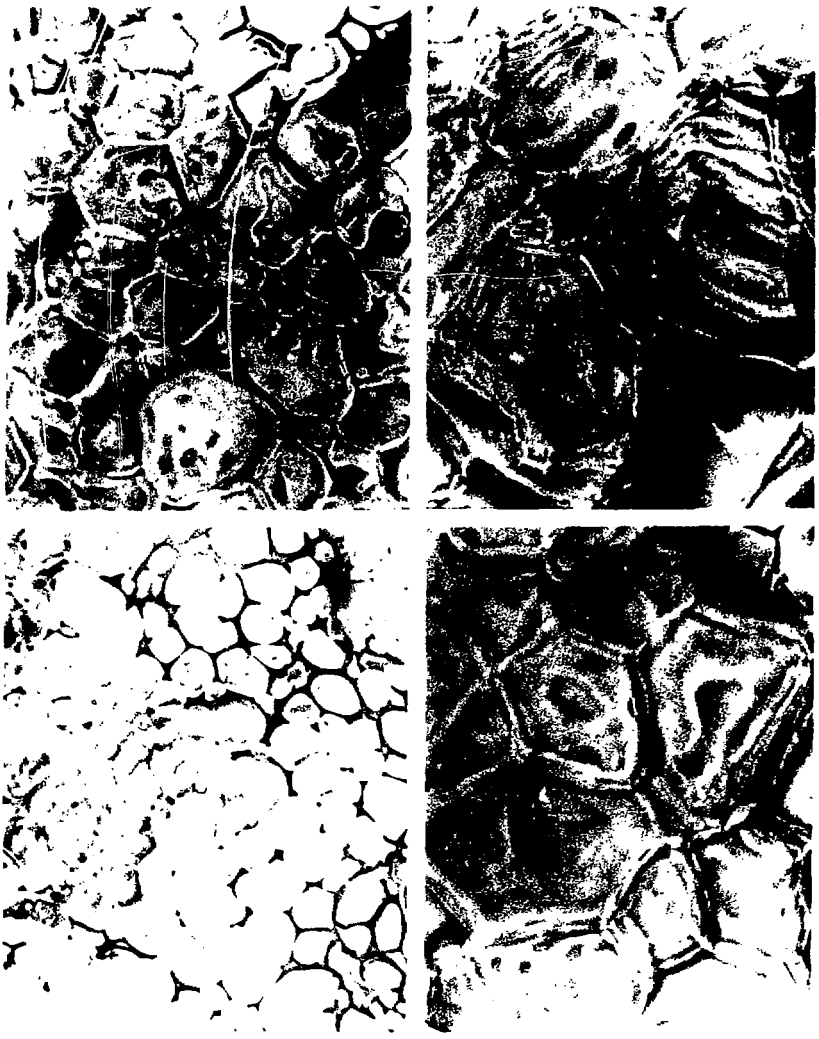

XBB789-12131

Fig. 3

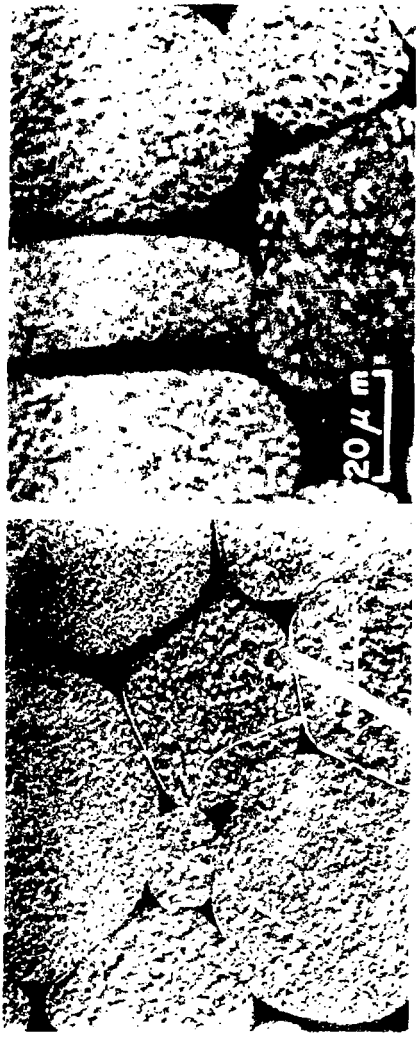

Fig. 4

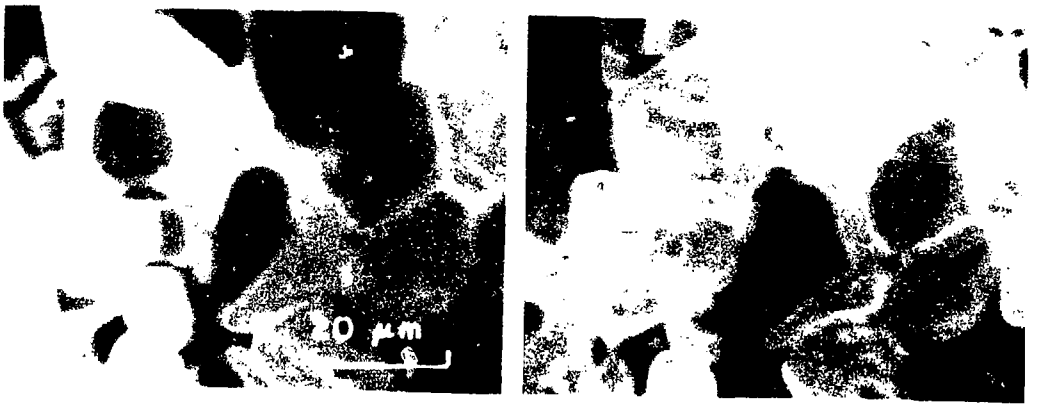

XBB789-12130

Fig. 5

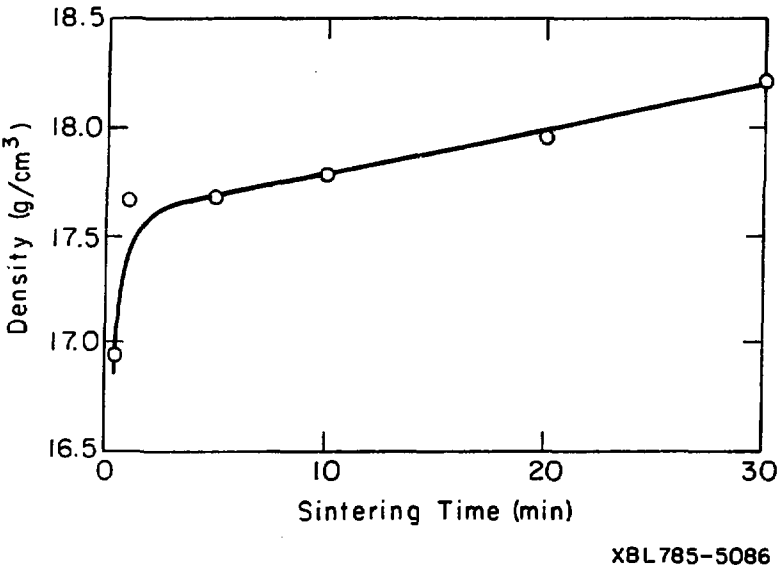
18.5
18.0
17.5
17.0
16.5
Density (g/cm^3)
0
10
20
30
Sintering Time (min)
XBL785-5086

Fig. 6

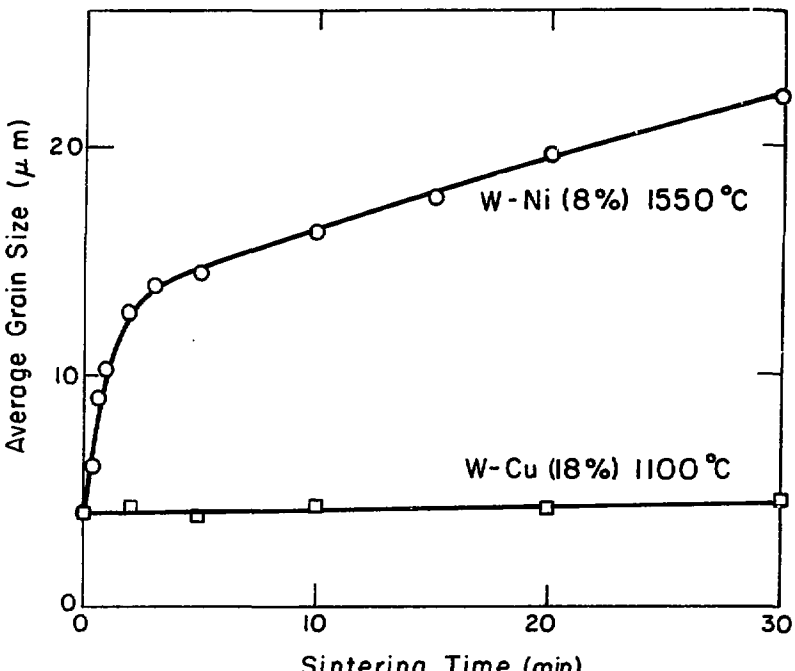

XBL 785-5085

Fig. 7

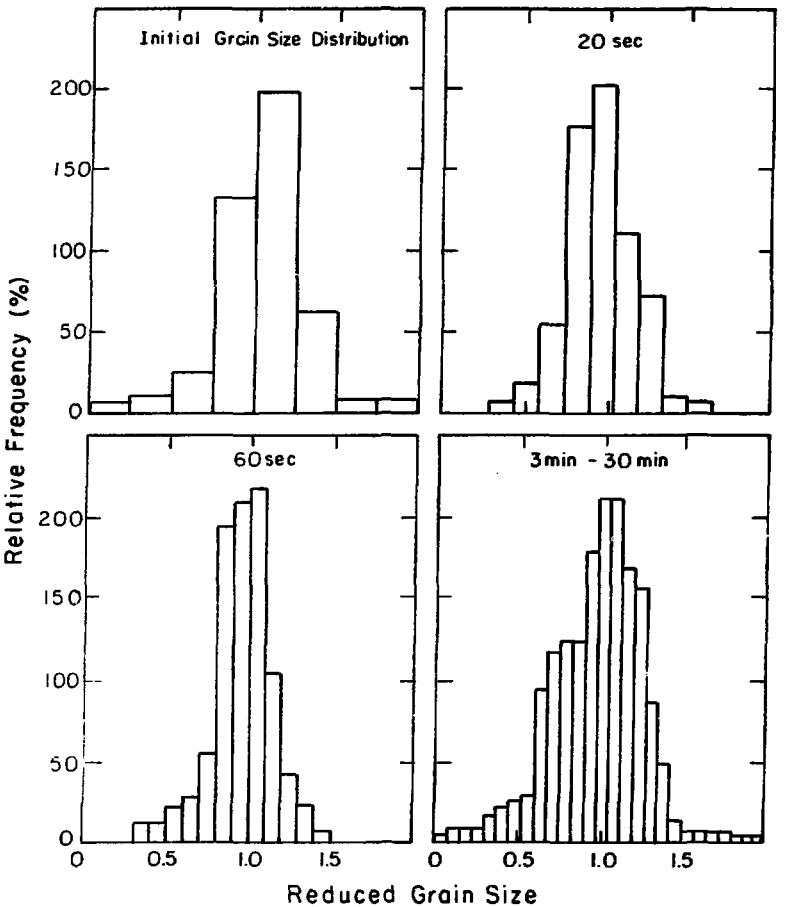

XBL 785-5084

Fig. 8

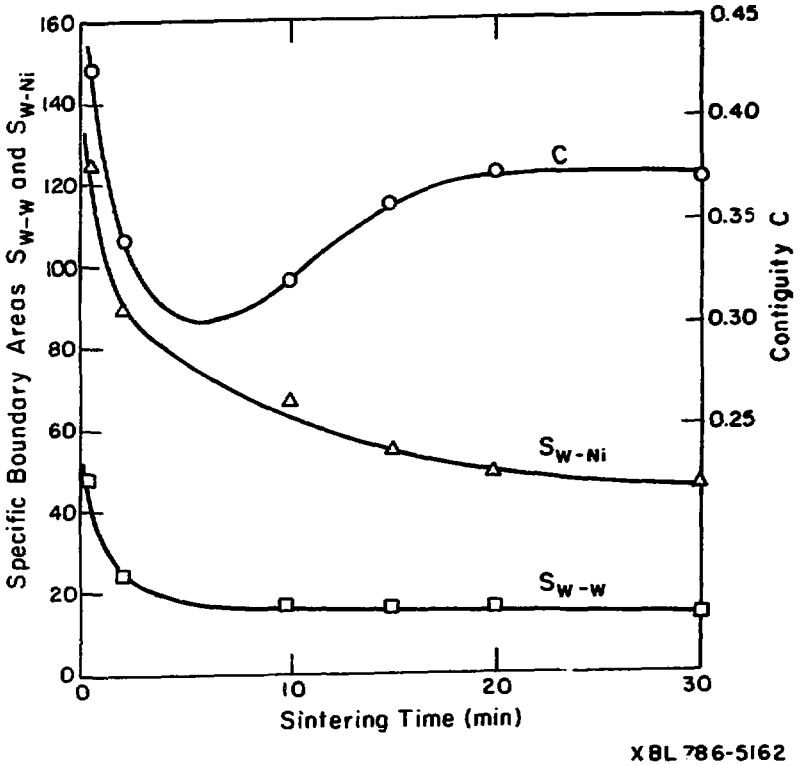
Specific Boundary Areas S_{W-W} and S_{W-Ni}
Contiguity C
Sintering Time (min)
C
S_{W-Ni}
S_{W-W}
160
140
120
100
80
60
40
20
0
0.45
0.40
0.35
0.30
0.25
0
10
20
30
XBL 786-5162

Fig. 9

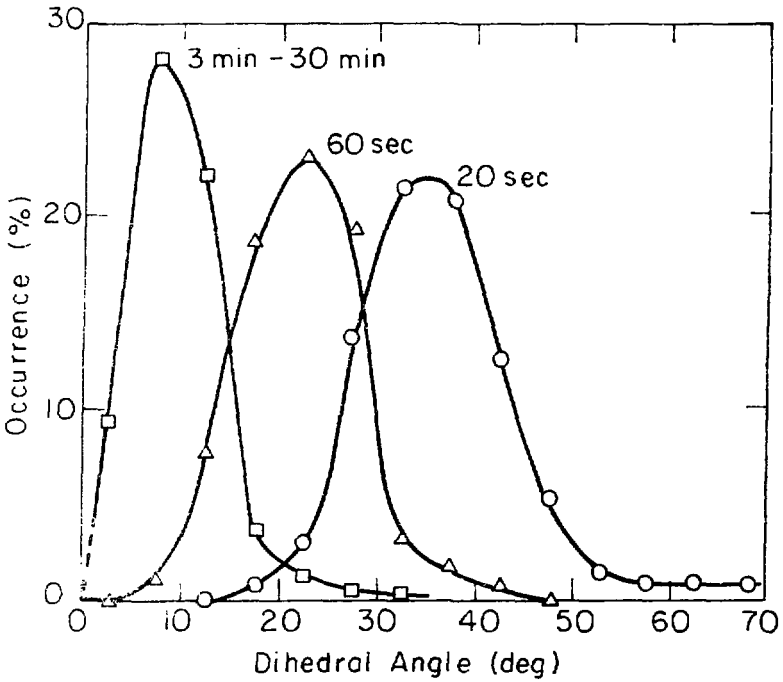

XBL785-5087

Fig. 10

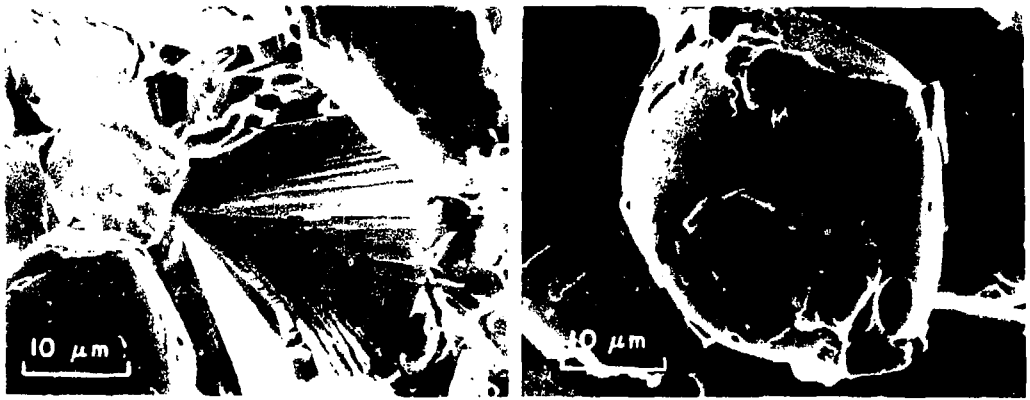

XBB789-12129

Fig. 11

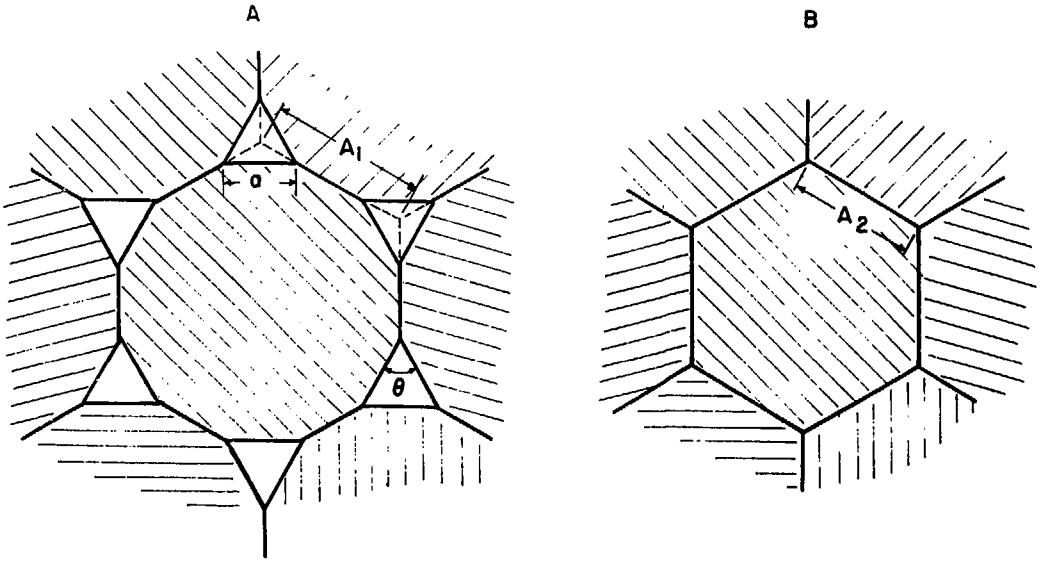

XBL 786-5186

Fig. 12

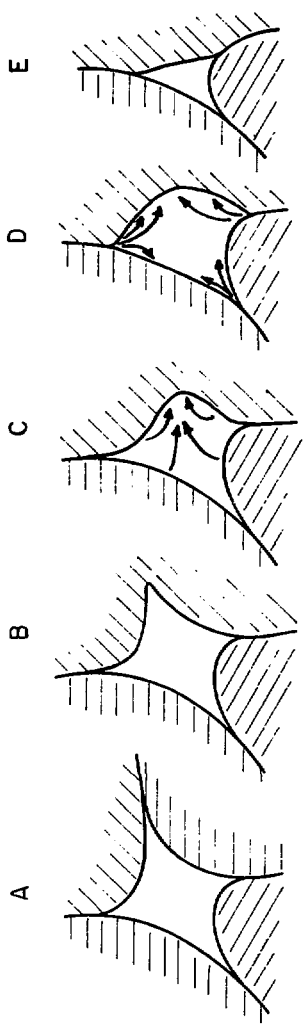

XBL 786-5185

Fig. 13

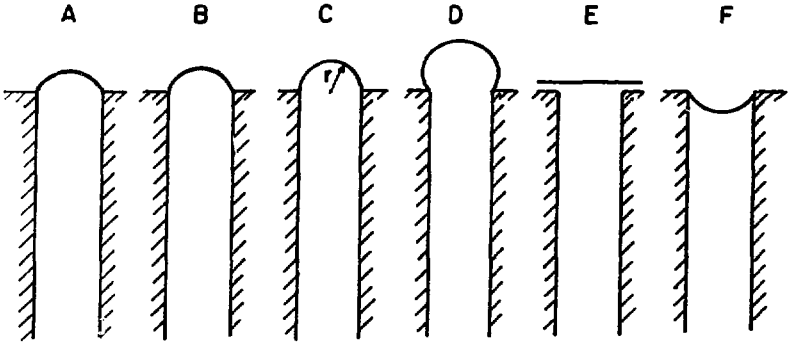

XBL 786-5187

Fig. 14

REFERENCES

1. G. H. S. Price, C. J. Smithells and S. V. Williams, "Sintered Alloys Part I. Copper-Nickel-Tungsten Alloys Sintered with a Liquid Phase Present," J. Inst. Met., 62, 239-264 (1938).
2. R. H. Krock, "Solid State Sintering and Particle Growth in Tungsten-Nickel-Iron Composite Material," Am. Soc. Test. Mater., 64, 669-680 (1964).
3. N. C. Kothari, "Densification and Grain Growth During Liquid Phase Sintering of Tungsten-Nickel-Copper Alloys," J. Less Common Met., 13, 457-468 (1967).
4. E. G. Zukas, L. S. Levinson, "Matrix Motion of Low Volume Matrix W-Ni-Fe Composites Sintered in a Temperature Gradient," J. Mat. Sci. 10, 863-869 (1975).
5. E. G. Zukas, H. Sheinberg, "Sintering Mechanisms in the 95% W - 3.5% Ni - 1.5% Fe Composite," Powder Technology, 13, 85-96 (1975).
6. E. G. Zukas, D. T. Eash, "Possible Reinforcement of the Tungsten-Nickel-Iron Composite with Tungsten Fibers," J. Less Common Met., 32, 345-353 (1973).
7. R. Watanabe, Y. Masuda, "The Growth of Solid Particles in Some Two Phase Alloys During Sintering in the Presence of a Liquid Phase," Materials Science Research, vol. 10, Sintering and Catalysis, ed. G. C. Kuczynski, Plenum Press, NY, London, 389-398 (1975).
8. E. G. Zukas, P. S. Z. Rogers, R. S. Rogers, "Spherical Growth by Coalescence during Liquid Phase Sintering," Z. Metallkde., 67, 591-595 (1976).

9. W. J. Huppmann, H. Riegger, "Liquid Phase Sintering of Model System W-Ni," Int'l. J. Powder Met. Powder Technol., 13, 243-247 (1977).

10. W. D. Kingery, "Densification During Sintering in the Presence of a Liquid Phase," J. Appl. Phys., 30, 301-310 (1959).

11. C. Wagner, "Theorie der Alterung von Niederschlaegen durch Umloesen (Ostwald-Reifung)," Z. Elektrochemie, 65, 581-591 (1961).

12. I. M. Lifshitz, V. V. Slyozov, "The Kinetics of Precipitation from Super Saturated Solid Solutions," J. Phys. Chem. Solids, 19, 35-50 (1961).

13. D. N. K. Wang, D. J. Miller, R. M. Fulrath, "Development of High Temperature Scanning Electron Microscopy and Applications to Sintering Studies," Scanning Electron Microscopy 1978, vol. 1, ed. O. Johari, 777-782 (1978).

14. H. Riegger, Ph.D. Thesis, "Verdichtungsmechanismen beim Sintern mit fluessiger Phase," University of Stuttgart (1977).

15. G. H. Gessinger, H. F. Fischmeister, "A Modified Model for the Sintering of Tungsten with Nickel Additions," J. Less Common Met., 27, 129-141 (1972).

16. H. E. Exner, H. L. Lukas, "The Experimental Verification of the Stationary Wagner Lifshitz Distribution of Coarse Particles," Metallography, 4, 325-338 (1971).

17. C. E. Hoge and J. A. Pask, "Thermodynamic and Geometric Considerations of Solid State Sintering," Ceramurgia Int'l., 3, 95-99 (1977).

18. P. Flaitz, University of California, Berkeley, private communication, 1978.

19. G. H. Gessinger, H. F. Fischmeister, H. L. Lukas, "A Model for Second Stage Liquid Phase Sintering with a Partially Wetting Liquid," Acta Met., 21, 715-724 (1973).

20. W. J. Huppmann, H. Riegger, "Modelling of Rearrangement Processes in Liquid Phase Sintering," Acta Met., 23, 965-971 (1975).